AN ABSTRACT OF THE THESIS OF

Sasi Kumar S. Arunachalam for the degree of Master of Science in
Electrical and Computer Engineering presented on August 24, 2005.
Title: An Efficient and Accurate Method of Estimating Substrate
Noise Coupling in Heavily Doped Substrates

Abstract approved: ───────────────────────────────────

Kartikeya Mayaram   Terri S. Fiez

This thesis presents a Z-parameter based model to predict the substrate noise coupling between two contacts in a heavily doped substrate for frequencies less than 2 GHz. The empirical model is scalable with contact size and spacings between the contacts and model parameters can be readily extracted from simulated or measured data. The error is within acceptable limits and computational costs associated with extraction of substrate parasitics is significantly reduced by using this model compared to numerical techniques. An application of the model to analyze the substrate noise coupling between a digital and analog block is also demonstrated.

An Efficient and Accurate Method of Estimating Substrate Noise Coupling in
Heavily Doped Substrates

by

Sasi Kumar S. Arunachalam

A Thesis

submitted to

Oregon State University

in partial fulfillment of
the requirements for the
degree of

Master of Science

Presented August 24, 2005
Commencement June 2006

Report Documentation Page	*Form Approved* *OMB No. 0704-0188*

Public reporting burden for the collection of information is estimated to average 1 hour per response, including the time for reviewing instructions, searching existing data sources, gathering and maintaining the data needed, and completing and reviewing the collection of information. Send comments regarding this burden estimate or any other aspect of this collection of information, including suggestions for reducing this burden, to Washington Headquarters Services, Directorate for Information Operations and Reports, 1215 Jefferson Davis Highway, Suite 1204, Arlington VA 22202-4302. Respondents should be aware that notwithstanding any other provision of law, no person shall be subject to a penalty for failing to comply with a collection of information if it does not display a currently valid OMB control number.

1. REPORT DATE **24 AUG 2005**	2. REPORT TYPE	3. DATES COVERED **00-00-2005 to 00-00-2005**
4. TITLE AND SUBTITLE **An Efficient and Accurate Method of Estimating Substrate Noise Coupling in Heavily Doped Substrates**		5a. CONTRACT NUMBER
		5b. GRANT NUMBER
		5c. PROGRAM ELEMENT NUMBER
6. AUTHOR(S)		5d. PROJECT NUMBER
		5e. TASK NUMBER
		5f. WORK UNIT NUMBER
7. PERFORMING ORGANIZATION NAME(S) AND ADDRESS(ES) **Oregon State University,School of Electrical Engineering and Computer Science,1148 Kelley Engineering Center,Corvallis,OR,97331-5501**		8. PERFORMING ORGANIZATION REPORT NUMBER
9. SPONSORING/MONITORING AGENCY NAME(S) AND ADDRESS(ES)		10. SPONSOR/MONITOR'S ACRONYM(S)
		11. SPONSOR/MONITOR'S REPORT NUMBER(S)

12. DISTRIBUTION/AVAILABILITY STATEMENT
Approved for public release; distribution unlimited

13. SUPPLEMENTARY NOTES

14. ABSTRACT

This thesis presents a Z-parameter based model to predict the substrate noise coupling between two contacts in a heavily doped substrate for frequencies less than 2 GHz. The empirical model is scalable with contact size and spacings between the contacts and model parameters can be readily extracted from simulated or measured data. The error is within acceptable limits and computational costs associated with extraction of substrate parasitics is significantly reduced by using this model compared to numerical techniques. An application of the model to analyze the substrate noise coupling between a digital and analog block is also demonstrated.

15. SUBJECT TERMS

16. SECURITY CLASSIFICATION OF:			17. LIMITATION OF ABSTRACT	18. NUMBER OF PAGES	19a. NAME OF RESPONSIBLE PERSON
a. REPORT **unclassified**	b. ABSTRACT **unclassified**	c. THIS PAGE **unclassified**	**Same as Report (SAR)**	**60**	

Master of Science   thesis   of   Sasi Kumar S. Arunachalam   presented   on

August 24, 2005

APPROVED:

_____

Co-Major Professor, representing Electrical and Computer Engineering

_____

Co-Major Professor, representing Electrical and Computer Engineering

_____

Director of the School of Electrical Engineering and Computer Science

_____

Dean of the Graduate School

I understand that my thesis will become part of the permanent collection of Oregon State University libraries. My signature below authorizes release of my thesis to any reader upon request.

_____

Sasi Kumar S. Arunachalam, Author

ACKNOWLEDGMENT

To my Parents

TABLE OF CONTENTS

TABLE OF CONTENTS (Continued)

LIST OF FIGURES

LIST OF FIGURES (Continued)

LIST OF TABLES

LIST OF APPENDIX TABLES

An Efficient and Accurate Method of Estimating Substrate Noise Coupling in Heavily Doped Substrates

1. INTRODUCTION

1.1. Background and Motivation

Continuous scaling of technology has resulted in system-on-chip (SoC) solutions for integrated circuits. These solutions are gaining popularity because of their numerous advantages in terms of reduced cost, size and improved performance. As a result, circuits with different functionalities are densely packed on the same substrate potentially resulting in unwanted interactions between them.

For example, in IC technologies analog and digital blocks are placed on the same silicon substrate. Substrate cross-talk between these blocks is a critical issue. As a result of the switching activity in the digital blocks, noise is injected into the substrate through parasitic capacitance coupling and bounce on the supply lines. This noise propagates through the substrate and changes the performance of the noise sensitive analog blocks through the body effect and capacitive coupling. A pictorial representation of the coupling mechanisms is shown in Figure 1.1. The noise injected into the substrate increases with an increase in the operating frequency and accurate characterization of the noise coupling is gaining importance. If these effects are not accurately accounted in the early stages of design, the design cycle time increases.

Although numerical methods [1, 2] are available to perform an accurate analysis of the substrate coupling, they are computationally expensive. The cost

increases with the transistors count thereby requiring an efficient alternative. Analyzing substrate coupling during post-layout stage leaves very few options for the designer to minimize the coupling. A pre-layout method of predicting the substrate coupling is desirable so that a designer can adopt noise minimization or isolation strategies. This provides the motivation for developing substrate coupling models that are scalable with the size and separations of contacts [3, 4]. Existing models [8] are accurate only for specific contact sizes and the error is unacceptable for the contact geometries not accounted while developing these models. This thesis presents a more general and accurate model for predicting substrate coupling in heavily doped substrates at low frequencies.
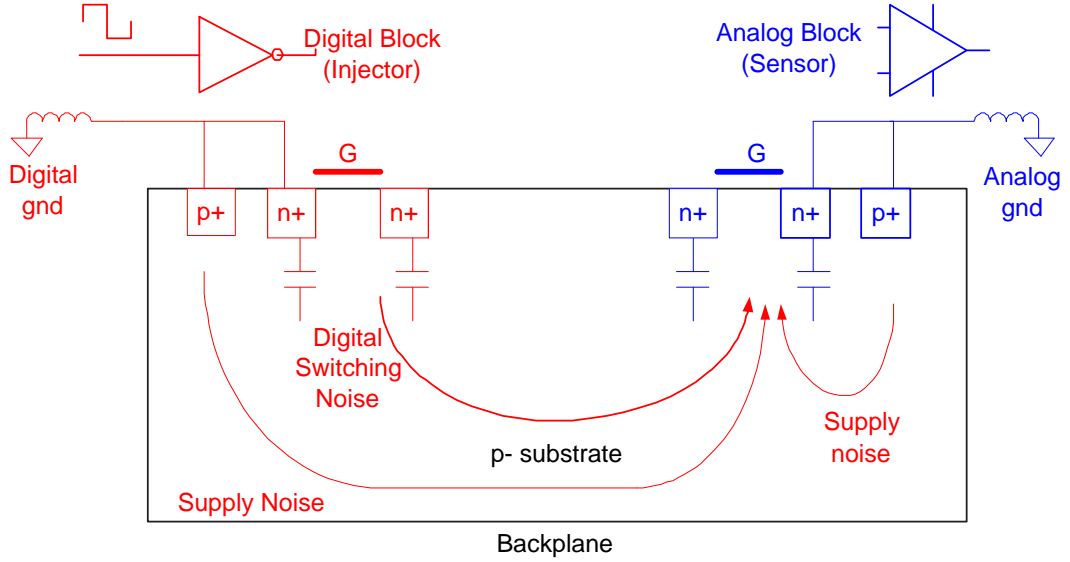
FIGURE 1.1. Substrate noise coupling mechanisms in a system-on-chip.

The thesis is organized as follows. A brief overview of previous work is provided in Chapter 2. Calibration of a simulator based on numerical methods is explained in Chapter 3. The results from the simulator are used to develop the model in Chapter 4. The model is validated with new test cases and results are summarized in Chapter 5. Finally, conclusions are drawn in Chapter 6.

2. OVERVIEW OF PREVIOUS WORK

This chapter discusses the advantages and disadvantages of analyzing substrate coupling using numerical methods and empirical models. The second half of the chapter deals with characterizing the substrate coupling using a π network of resistors.

2.1. Numerical Techniques

Various numerical techniques available for analyzing substrate noise coupling can be broadly divided into two types, namely the *finite element method* (FEM) and the *boundary element method* (BEM). The classical finite element methods divide the entire three-dimensional volume of the substrate and contacts with a mesh and solve Poisson's equation [5]. These methods are versatile since they can account for any changes in substrate resistivities in lateral or vertical directions. However, they are computationally expensive in terms of time and memory requirements.

On the other hand, the boundary element methods use a 2-D discretization of the surface contacts into panels and solve an equivalent integral form of the equations [5]. These methods assume a finite number of layers of uniform resistivity for the substrate. Hence these methods are computationally efficient compared to the FEMs.

The boundary element methods are also not suitable when the number of contacts increase to several thousands as in a real mixed-signal system. The process of extracting the substrate resistances involves an inversion of the panel level matrix. As the number of panels increase, the computation cost associated with matrix inversion becomes unacceptable. For example, a test case containing

a two-stage opamp and a stepped buffer with two guard rings had a total of only 95 contacts. A Green function solver took about 3 hours to extract the substrate network for this problem.

2.2. Empirical Models

Empirical parametric models can be obtained by curve fitting simulation or measured data. These models relate the substrate parasitics to the contact geometries and separation. Since extraction of the substrate parasitics requires evaluation of expressions, these models are several orders of magnitude faster than simulations [7]. Also, these models provide more insight into placement of various blocks during floorplanning. But assumptions are made while developing these models and there could be accuracy issues for the cases where these assumptions do not hold [8]. Hence, there exists a trade-off between the accuracy of numerical methods and the efficiency of empirical models.

2.3. Substrate Coupling Network

Silicon substrates can be broadly divided into two types, namely lightly doped and heavily doped substrates. Typically the heavily doped substrates can be represented by a three layered approximation of the actual doping profile. Typical values for the thickness and resistivity for each layer are shown in Figure 2.1. The first layer is a thin channel stop layer. The second layer is a high resistive epitaxial layer used to avoid latch-up problems [9]. This is followed by a thick low resistivity bulk layer. The heavily doped bulk can be treated as a single node [10]. Hence, noise injected into the bulk can be readily picked up across the entire die and there is larger noise coupling compared to a lightly doped substrate. For this

5

reason, heavily doped substrates are not preferred for low noise applications. For frequencies below 2 GHz, the substrate can be characterized by resistive networks [9] due to the low permittivity of silicon.

Channel Stop	p 1 ohm-cm	1 um
Epitaxial	p- 10 ohm-cm	10um
Bulk	p+ 1m ohm-cm	300um
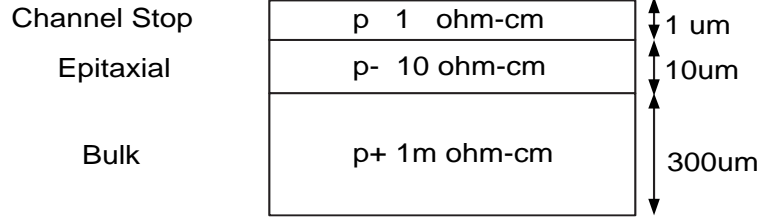
FIGURE 2.1. A typical three-layer approximation derived from the doping profile of a heavily doped silicon substrate.

To characterize the coupling between two contacts, open circuit impedance Z parameters are used [11]. For any two contacts in the substrate, the system of equations is as follows:

$$[V] = [Z] \, [I]$$

where V is the vector of contact potentials, I is the vector of currents injected into the contact and Z is the open circuit impedance matrix. The Z parameters for two contacts, namely contact-i and contact-j are

$$\begin{bmatrix} V_i \\ V_j \end{bmatrix} = \begin{bmatrix} Z_{ii} & Z_{ij} \\ Z_{ji} & Z_{jj} \end{bmatrix} \cdot \begin{bmatrix} I_i \\ I_j \end{bmatrix} \tag{2.1}$$

The self impedance Z_{ii} is the potential on contact-i when a unit current is injected into contact-i with contact-j as an open circuit. The mutual coupling parameter Z_{ij} is the potential at the floating contact-i when a unit current is injected into contact-j. By the reciprocity principle, $Z_{ij} = Z_{ji}$. These Z parameters vary with the sizes and separation of the two contacts.

The advantage of using Z parameters is that the Z parameters for any two contacts can be extracted independent of the other contacts. This is because the

other contacts surrounding the two contacts should not affect the two contact Z parameters since the other contacts are left floating [12].

The substrate coupling network can be represented as a π network as shown in Figure 2.2. Each contact has a self coupling resistor R_{ii} to the backplane and a cross coupling resistor R_{ij} to each of the other contacts.
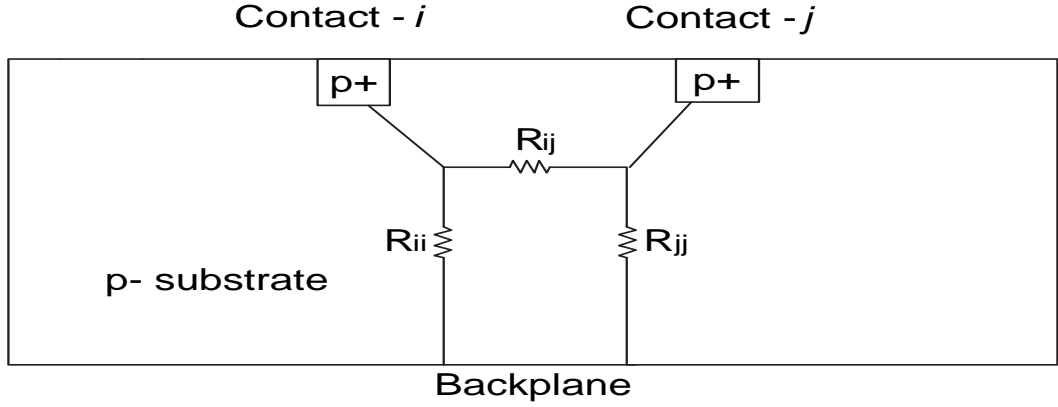
FIGURE 2.2. π model for the substrate coupling network.

To obtain the substrate resistance network, the Z parameters must be converted into resistors. The Z matrix is inverted to obtain the admittance matrix Y. The substrate resistances are computed using Eq. (2.2).

$$R_{ii} = \frac{1}{\sum_j Y_{ij}} \qquad\qquad R_{ij} = -\frac{1}{Y_{ij}} \qquad\qquad (2.2)$$

A model can be developed to obtain the Z parameters for two contacts. The substrate resistances can then be extracted using Eq. (2.2). These can be combined with a circuit for analyzing the substrate noise coupling.

3. CALIBRATION

Models can be developed by curve fitting to measured or simulated data. To obtain an accurate model for any contact size and spacing, sufficient data is required. Measured data for these cases involves the cost of fabricating a large number of test structures. These test structures can be simulated using numerical methods and the required data can be obtained in a cost effective manner. The latter approach works only when the simulated data matches the data expected from measurements.

As explained in Section 2.1, a Green function based substrate network extractor requires the substrate to be divided into a finite number of layers of uniform resistivities as shown in Figure 2.1. The actual doping profile needs to be approximated to obtain a profile similar to that in Figure 2.1. The extracted substrate parasitics are very sensitive to the substrate profile. The resistivities and the thickness of the substrate layers used for a Green function solver need to be optimized so that the extracted substrate parasitics match the measurement results. This procedure is referred to as a calibration step for the Green function solver [8].

In [8], the calibration for a 3-layered substrate is performed using measurement results for 8 test structures. In this work a detailed analysis is carried out for the number of substrate layers and sizes of test structures required for calibration. These two inputs to the calibration step determine the accuracy and computational cost of substrate parasitic extraction. The performance characteristics of the calibration methodology are optimized by using an optimum number of substrate layers and test structures.

3.1.   Choosing the number of substrate layers

It may be possible to improve the accuracy of the extracted substrate parasitics by using a finer resolution for the substrate (e.g., 5 or 7 layers) at the cost of increased computation time. For example, let us consider a test case containing an opamp and a stepped buffer. The two circuits have a total of 45 contacts. The coupling network extraction time using a 7-layered substrate is 164 minutes as compared to 25 minutes using a 3-layered substrate. In this section, the trade-off between the accuracy and efficiency of substrate parasitic extraction is discussed.
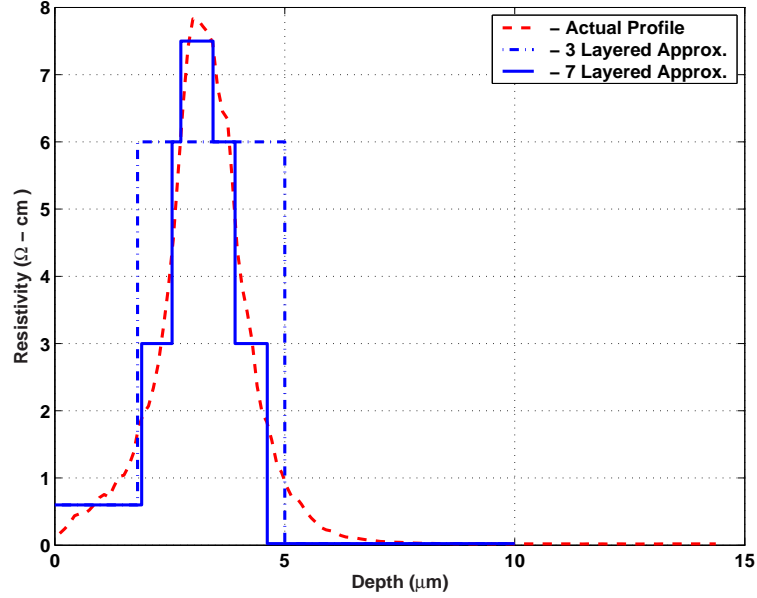
FIGURE 3.1. Actual and approximated resistivities for a heavily doped substrate.

First we consider the use of 5 or 7-layer approximations without the use of a calibration step. A 3- and 7-layer approximation of the actual substrate resistivity is shown in Figure 3.1. The substrate parasitics are extracted using non-calibrated profiles for 3, 5 and 7-layer approximations of the substrate doping and compared with measured results. The results are summarized in Figure 3.2.

It is seen that the 5 or 7 layered non-calibrated substrate profiles do not match the measured data and are no more accurate than the non-calibrated 3 layered approximation.
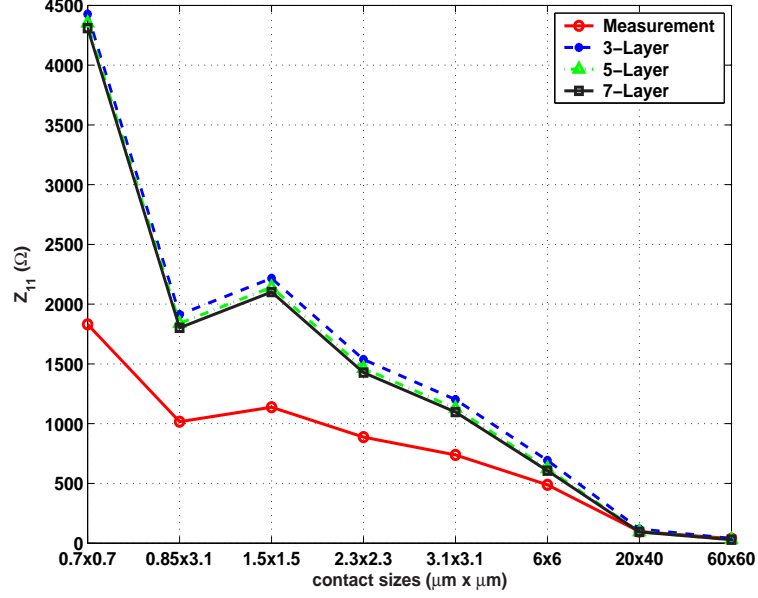
FIGURE 3.2. Z_{11} extracted using non-calibrated profiles for 3, 5 and 7 layers.

Next the calibration procedure is repeated for the 5- and 7-layer approximations of the substrate. The accuracy of the calibrated 5- and 7-layer profiles is similar when compared with the 3-layer approximation. However, the computational cost increases significantly. The calibration time for 3-, 5- and 7-layer approximations is 2.5, 47 and 94 hours, respectively on a Sun Ultra 10 processor.

The calibration procedure should allow for an accurate extraction of the parasitics with minimum computational cost. The additional complexity and computational resources resulting from the additional layering of the substrate outweighs the small improvement in accuracy. For these reasons, the 3-layered substrate serves as a good approximation for the heavily doped cases.

Although the 3-layer calibration requires about 2.5 hours on a Sun Ultra 10 processor, this is done only once for a particular IC process. Once the substrate has been calibrated, all subsequent parasitic extraction with the Green function solver using the calibrated substrate profile are accurate.

3.2. Choice the sizes of test structures

Another input to the calibration procedure that affects the trade-off between the accuracy and cost of substrate extraction is the number of test structures. In this case, the cost includes the fabrication of the test structures. The test structures used for calibration affect the accuracy of the extracted parasitics.

A layout will typically have square and rectangular shaped contacts. For this reason, the calibration test structures should include both square contacts with small (e.g., 0.7 μm x 0.7 μm) and large (e.g., 60 μm x 60 μm) sizes and rectangular contacts with small (e.g., 0.85 μm x 3.1 μm) and large (e.g., 20 μm x 40 μm) dimensions.

For the 3-layer substrate, the profile was calibrated using only these 4 test structures. The Z_{11} values obtained from the calibrated profile from these test structures is shown in Figure 3.3 and these are in close agreement with those in the previous work of [8] with 8 test structures. Hence, we can obtain sufficiently accurate results with a minimum of 4 contacts.
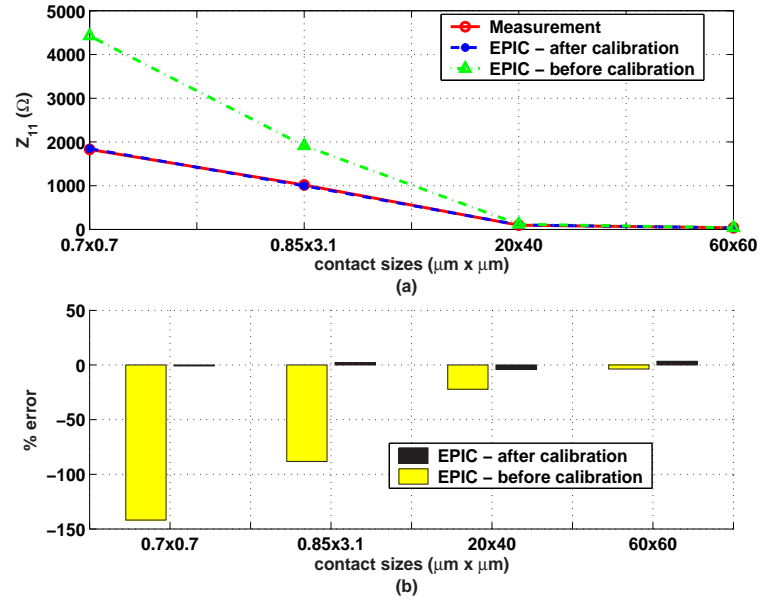
FIGURE 3.3. Calibration of Z_{11} with only 4 test structures. (a) Values of Z_{11} before and after calibration. (b) Percentage error relative to measurements for the test structures used for calibration.

4. EMPIRICAL MODEL

This chapter describes the development of a model for determining the Z parameters for two contacts. The simulation results from a calibrated extractor are used for model development and verification.

4.1. Existing Model and its Limitations

Since Z parameters for a single contact are assumed to be independent of other contacts, the self impedance parameter Z_{ii} is modeled as a function of the geometry of contact-i in [11]. The model for Z_{ii} is given in Eq. (4.1).

$$Z_{ii} = \frac{1}{k_1 A_i + k_2 P_i + k_3} \tag{4.1}$$

where A_i and P_i are the area and perimeter of contact-i and k_1, k_2 and k_3 are process related constants.

In [8], more work was done in modeling the mutual coupling parameter Z_{ij}. The separation along the x and y axes was defined as shown in Figure 4.1 for a two contact problem. The distance d_x is the edge-to-edge separation between the two contacts whereas the distance d_y is the center-to-center separation between the two contacts.

The model was developed by curve fitting measurement data since EPIC was not calibrated at that time. Very few combinations of two contact sizes and separations were fabricated and measured. As a result, the model gives unacceptable error for other cases. Also, the model has large number of process related constants due to the use of separate models for small and large separations. A calibrated extractor allows one to test a large number of two contact problems
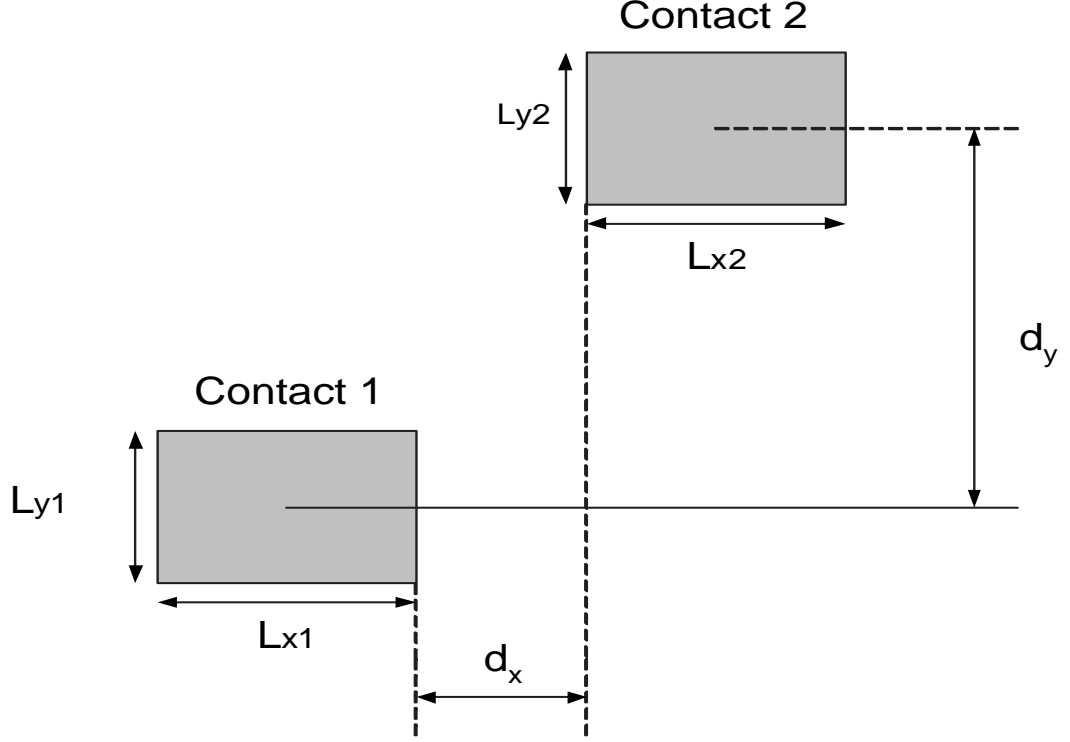
FIGURE 4.1. Convention of x and y separation between two contacts.

of different sizes and separations without the need for fabrication. This helps in developing a more robust model with high accuracy.

4.2. Geometric Mean Distance

As seen in the previous section, defining the separations along both the x- and y- axes separately leads to an increase in the number of model parameters. Alternatively, for any two contacts, the separation can be efficiently represented by the geometric mean distance (GMD) between them. The GMD (D_{ij}) between two contacts (i, j) of areas A_i and A_j is given by Eq. (4.2) [13].

$$lnD_{ij} = \frac{1}{A_i A_j} \int_{A_i} \int_{A_j} ln\, d\, dA_j\, dA_i \qquad (4.2)$$

where d is the separation between any two points on the two contacts. In [14], an approximation of the GMD is used to model the cross-coupling resistance in lightly doped substrates. The use of the GMD for modeling the mutual coupling parameter Z_{ij} of two contacts in heavily doped substrates is examined in the following subsection.

4.2.1. Analysis of simulation results

The objective is to check if Z_{ij} is a unique function of GMD for all combinations of two contacts geometries in a heavily doped substrate. To check this, three different cases are considered for varying the separation, namely along the X-axis, the Y-axis and the XY-direction. Distances d_x and d_y are separations as defined in Figure 4.1. The three cases are as follows:

- The separation along the X-axis d_x, is varied from 1 to 50 μm while d_y is kept constant at 0 i.e., the centers of the two contacts are aligned.

- The separation d_x is fixed, at say 2 μm. While d_y is varied from 1 to 50 μm.

- Both the separations d_x and d_y are varied equally from 1 to 50 μm.

Eight different combinations of two contacts including squares, rectangles with different aspect ratios (lx/ly) have been considered. The contact sizes are listed in the APPENDIX A. The above three cases are simulated using EPIC for the 8 two-contact problems. The GMD given by Eq. (4.2) can not be computed analytically. A numerical integration is used to evaluate this expression.

If Z_{ij} is only a function of GMD as identified in [14], then for different separations along the X, Y and XY-directions, Z_{ij} must be the same for a given GMD.
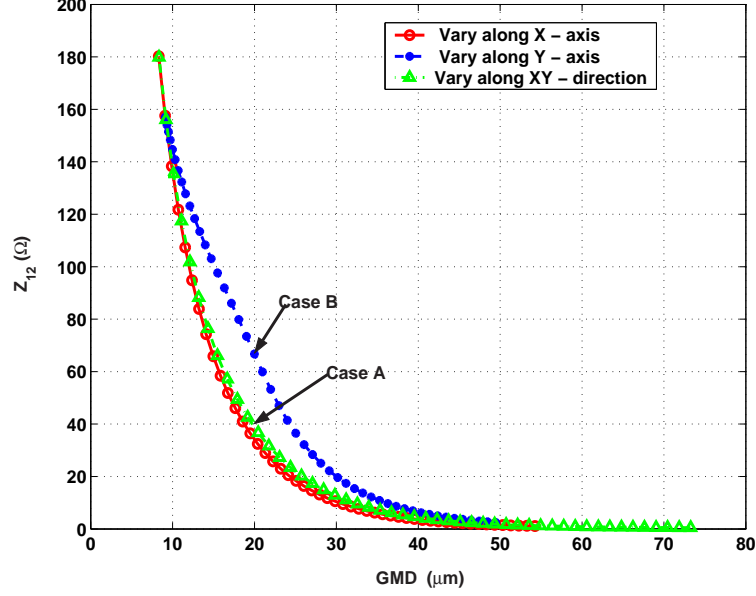
FIGURE 4.2. Plot of Z_{ij} values from EPIC as a function of GMD.

A plot of Z_{ij} vs. D_{ij} is shown in Figure 4.2. As can be seen in this figure, the data for X and XY separations give the same value for Z_{ij} for a given D_{ij}. For Y separation, this occurs only at the two extreme separations. The difference in Z_{ij} values compared with the previous two cases increases to a maximum value for a particular D_{ij} and then decreases finally becoming negligible.

The above behavior can be explained as follows. For small values of d_y, the d_x and d_y values are comparable in all the three cases and so the mutual coupling between the two contacts is similar. For large values of d_y, most of the injected current flows to the backplane. The mutual coupling is very weak and does not depend on the separation. This results in the same value for Z_{ij} for all of the three cases for large GMD values.

To understand the simulation results for the separation where the devia-
tions are significant, consider a numerical example. Two data points are marked
in Figure 4.2. Case A corresponds to a data point in the test suite varying the
separation along the X axis, namely $d_x = 15~\mu$m. Similarly, case B corresponds to
a data point in the test suite varying the separation along the Y axis, namely $d_y =$
21.5 μm. The graphical representation for these two cases is shown in Figure 4.3.
For both these cases, the GMD is calculated to be 20 μm. But the simulated
Z_{ij} is 40Ω and 65Ω, respectively. This is because in case B, the two contacts are
physically closer than in case A even though the GMD remains the same. For
the contacts in case B the mutual coupling is larger and this explains the trend
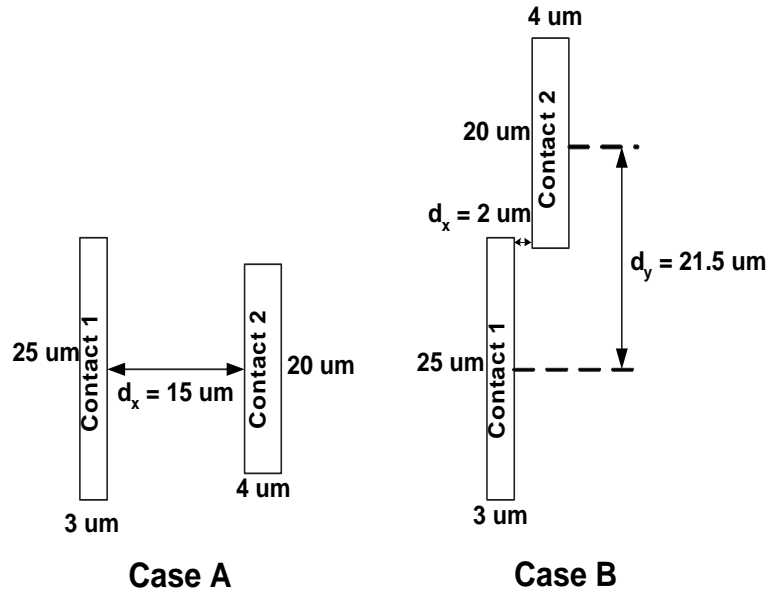observed in the Z_{ij} values.

FIGURE 4.3. Graphical representation of the test cases A and B considered in
Figure 4.2.

From these experiments, it is noted that Z_{ij} is a stronger function of separa-
tion along the x axis. The GMD concept does not consider the x and y separations

in a unique manner. The deviation in Z_{ij} values increases with an increase in the contact dimensions along the y axis (ly). This study reveals that Z_{ij} can not be modeled as a function of the GMD in heavily doped substrates. Both the x and y separations need to be accounted for.

Selecting an appropriate definition for separation is important in developing the model for mutual coupling. The separation along the x axis is defined as the edge-to-edge separation as opposed to center-to-center separation because the latter characterizes the mutual coupling more accurately than the former.

For variation of separation along the y axis, the coupling is symmetric about the point where the centers of the two contacts are aligned. For convenience, the center-to-center separation is chosen for the y axis. For these reasons, the separations used in this work are the same as those in [8] and as shown in Figure 4.1.

4.3. Model for x-separation

A model is developed to predict the coupling between two contacts for varying separation along the x axis. Simulation results obtained using EPIC are used to develop the model.

4.3.1. Analysis of simulation results

The cross coupling parameter Z_{ij} has been extracted for two identical square contacts of size 10 μm for various d_x values from 1 μm to 300 μm. The resulting Z_{12} values are plotted in Figure 4.4(a). It can be seen that the mutual coupling decays exponentially with an increase in the separation. The results with a natural logarithmic scaling for the y axis are shown in Figure 4.4(b)and

two distinct slopes are observed. Two exponential functions are required to model the complete behavior of Z_{12}.
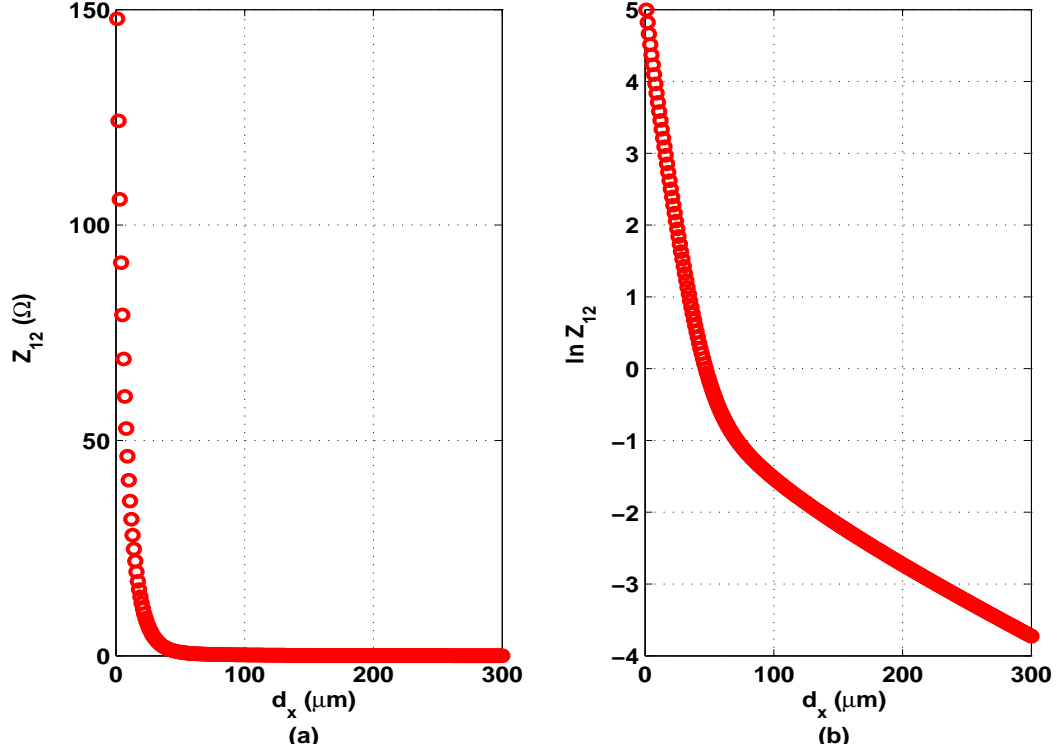
FIGURE 4.4. Plot of EPIC values for Z_{12} as a function of d_x (a) Regular scaling, and (b) log_e scaling for the y axis.

For a large N-contact problem, an acceptable error in Z-parameter values could translate into an unacceptable error in resistor values after matrix inversion [15]. Eventually, resistors values are used for substrate noise analysis. So, it is very important to model the entire behavior of Z_{ij} in Figure 4.4 accurately. This resulted in a large number of parameters due to two exponential functions.

4.3.2. Ratio-Accelerated Technique

To reduce the computational cost in inverting dense matrices, a technique called the ratio-accelerated technique [12, 16] is used. In this technique the

small entries in an impedance matrix (due to contacts that are distant from one another) are neglected. This approach is applicable for heavily doped substrates since Z_{ij} decreases rapidly with separation. Beyond a certain separation between two contacts, the Z_{ij} entry in the impedance matrix can be neglected. A threshold value is used to ignore the relatively small Z_{ij} values. The threshold is defined as the ratio of the mutual impedance to the self impedance (i.e., Z_{ij}/Z_{ii}).
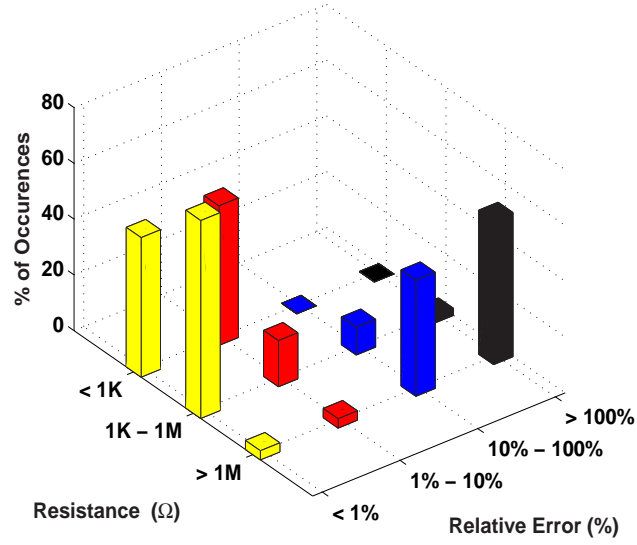
FIGURE 4.5. Histogram of error in each range of resistor values.

To study the performance of this technique against the observation in [15], two different examples were considered. In one case, the setup included a stepped buffer as a noise injector and a folded cascode opamp as the noise sensitive block. In the second case the noise sensor is a two stage opamp and both the injector and sensor blocks are surrounded by guard rings. Since these examples are from a test chip, the contact sizes and spacings are typical values in a layout. The two cases had 55 and 95 contacts, respectively. The Z and R matrices were extracted from EPIC simulations.

All Z_{ij} entries below 2Ω are neglected and a new R matrix is computed as explained in Section 2.3. The error in the new R matrix is computed relative to the simulated R matrix. For cross-coupling resistors (R_{ij}) below 1KΩ, the error was less than 10% (Figure 4.5). Only resistors R_{ij} above 1MΩ had significant errors as stated in [15].

In heavily doped substrates, the resistance to the backplane is the major path for noise coupling for separations beyond a critical distance given by 4 times the thickness of the epitaxial layer (t_{epi}) [17]. For these distances, the coupling between contacts is independent of the mutual coupling resistor R_{12}. The substrate noise analysis results are least affected by errors in large resistors. Hence the model could be simplified by neglecting the Z_{ij} behavior for large separations. This allows us to use a single exponentially decreasing function of separation for modeling Z_{12} with a reduced number of parameters.

4.3.3. Model Development

To develop a model valid for any contact geometries, an appropriate list of test structures has been developed. It includes square contacts of small and large sizes and rectangular contacts of small and large dimensions. All of the two contact combinations in this list were simulated in EPIC for d_x ranging from 1 μm to 45 μm. The two contacts are symmetrically placed in the center of a 1000 μm X 1000 μm die to avoid edge effects [12]. At $d_x = 45$ μm, the Z_{ij}'s are in the order of 1-2Ω for all the test cases. Therefore, the mutual coupling between two contacts can be neglected for separations greater than 45 μm.

An exponentially decreasing function of separation is used to model the mutual coupling parameter. The expression is modified as shown in Eq. (4.3) so

that the error is within 10% for all the cases with separations between 2 μm and 45 μm. The model parameters α_{ij} and β_{ij} are dependent on the geometries of the two contacts. The comparison between the model given by Eq. (4.3) and EPIC results is shown in Figure 4.6 for 3 test cases.

$$Z_{ij} = \alpha_{ij} \; exp(-\beta_{ij} \, d_x^{\;0.75}) \qquad (4.3)$$
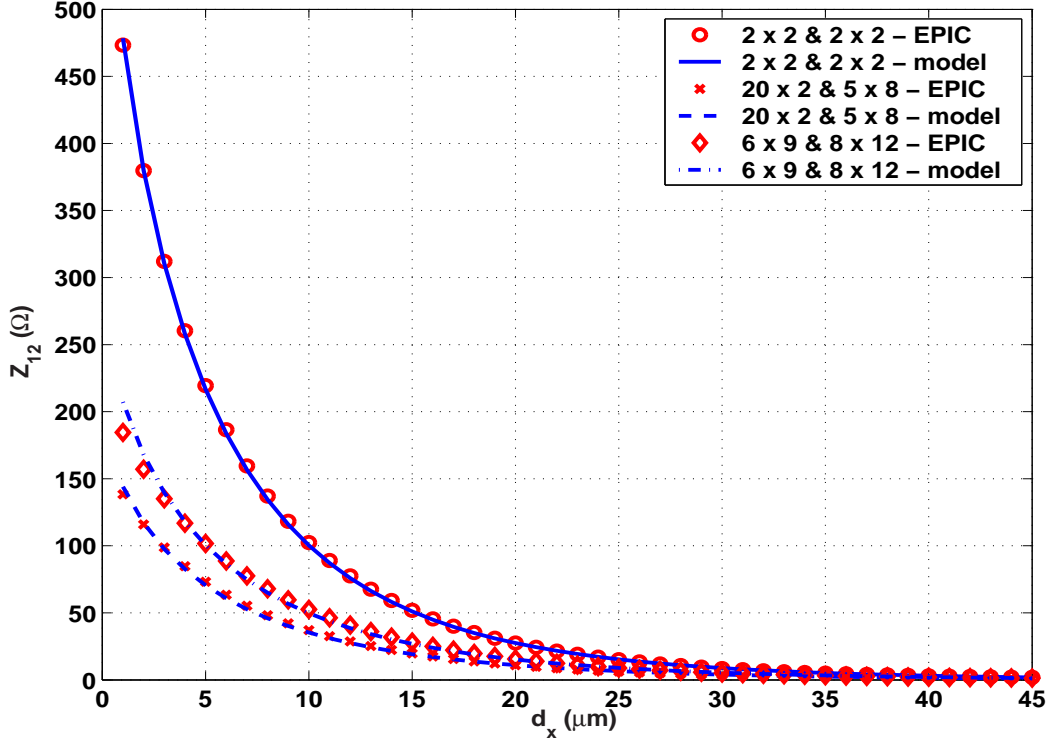
FIGURE 4.6. Comparison of the model for Z_{ij} and EPIC results.

At zero separation ($d_x = 0 \; \mu$m), the two contacts are merged into a single contact. This merged contact is a single port and it essentially has only one Z parameter, namely the Z_{ii} of the merged contact. Theoretical expectations reveal that Z_{ij} at zero separation must be equal to the Z_{ii} of the merged contact [18].

For a two contact case, the relation between the Z parameters and resistors are given by Eqs. (4.4) and (4.5).

$$Z_{11} = R_{11} \| (R_{12} + R_{22}) \tag{4.4}$$

$$Z_{12} = \frac{R_{11} \times R_{22}}{R_{11} + R_{12} + R_{22}} \tag{4.5}$$

As $d_x \to 0$, $R_{12} \to 0$, Eqs. (4.4) and (4.5) reduce to Eq. (4.6).

$$Z_{11} = Z_{12} = Z_{22} = R_{11} \| R_{22} = Z_{11} \text{ of the merged contact.} \tag{4.6}$$
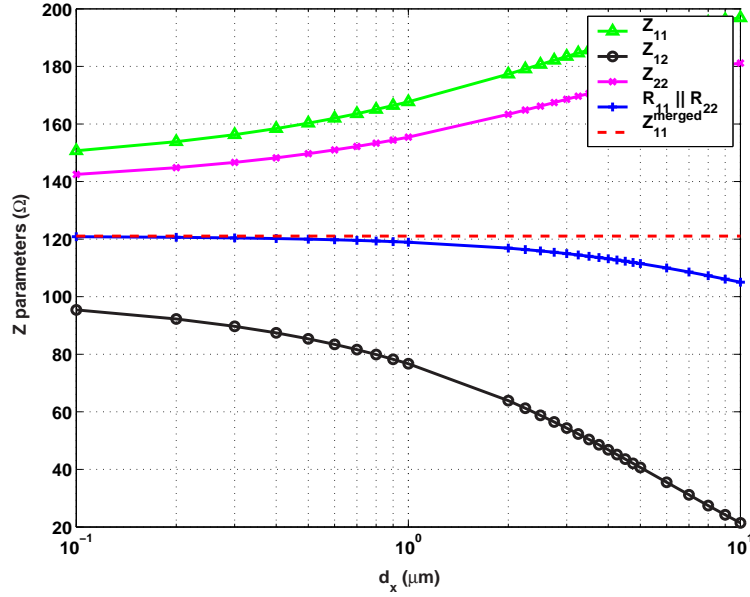
FIGURE 4.7. Two port Z-parameters at small separations.

Eq. (4.6) has been verified with EPIC results as shown in Figure 4.7. From Eq. (4.3), Z_{ij} at $d_x = 0$ μm reduces to α_{ij}. However, the extracted values for α_{ij} in the model do not match the Z_{ii} of the merged contact as expected from Eq. (4.6). To analyze the deviation, EPIC simulations were performed for separations between 0.1 μm and 5 μm. Since the two contacts are very close to each other, the contacts need to be divided into smaller panels to account for the proximity effect [6].

Modeling the Z_{ij} at small separations gets complicated and leads to additional parameters. The model given in Eq. (4.3) is valid for separations larger

than 2 μm. Separations below 2 μm are not frequently encountered due to fabrication process specifications. So it is not necessary to model the coupling at separations below 2 μm. Eq. (4.3) efficiently models the mutual coupling in the desired separation range, obviating the need for a separate model for near and far field effects as in [19]. The Z_{ii} of the merged contact can not be used for the α_{ij} parameter. Hence, a different model is required for α_{ij} parameter.

The parameter α_{ij} needs to be modeled as a function of the geometries of contact-i and contact-j. The geometries of the two contacts need to be uniquely defined in an efficient manner to obtain an accurate model for α_{ij}. Use of the contact perimeter and area in the model yields errors that are large. This is because these variables do not contain information about the contact orientation. The dimensions along the x and y axis are not uniquely specified. For example, consider two cases as shown in Figure 4.8. In both the cases, the dimensions of the second contact is fixed, say 2 μm x 2 μm. The first contact is 20 μm x 2 μm in the first case and 2 μm x 20 μm in the other. The first and second contacts in both the cases have the same area and perimeter values. However, the coupling between the two contacts is different, resulting in significantly different Z_{ij} and α_{ij} values. For this reason, the orientation of the two contacts is important in modeling the mutual coupling. The lengths of the two contacts in the x and y directions need to be included.

As discussed in Chapter 2, the mutual coupling between the contacts is reciprocal in nature i.e. Z_{ij} is equal to Z_{ji} implying α_{ij} is equal to α_{ji}. The model given by Eq. (4.7) satisfies this condition.

$$\alpha_{ij} = \frac{1}{c_1(Lx_i + Lx_j)^{c_2} + c_3(Ly_i + Ly_j)^{c_4} + c_5(Lx_i + Lx_j)(Ly_i + Ly_j) + c_6} \quad (4.7)$$
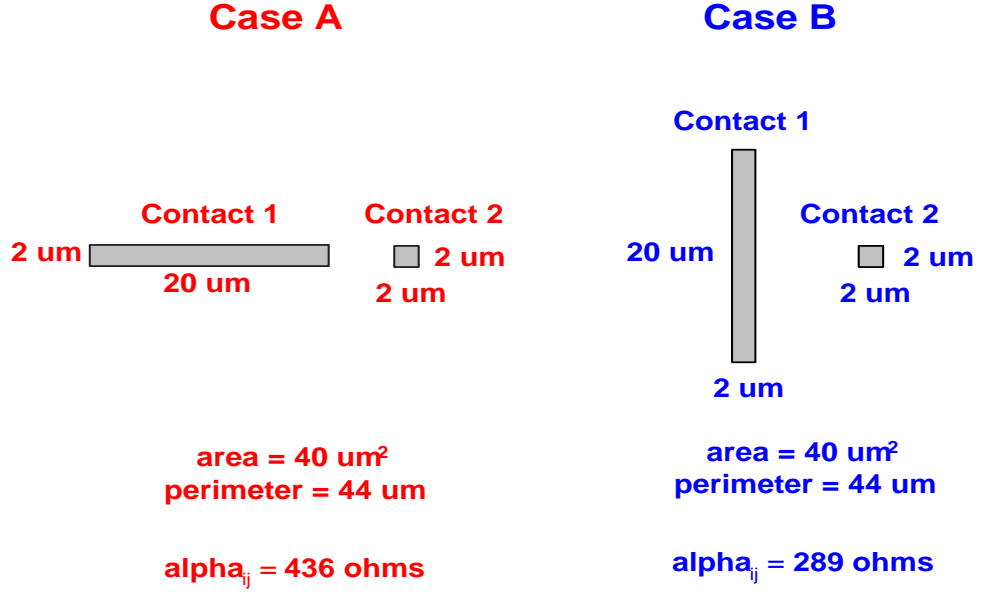
Case A **Case B**

Contact 1

Contact 1 **Contact 2**

2 um | **2 um** **20 um** **Contact 2**

20 um **2 um** **2 um**

2 um **2 um**

2 um

area = 40 um²
perimeter = 44 um

area = 40 um²
perimeter = 44 um

alpha$_{ij}$ = 436 ohms

alpha$_{ij}$ = 289 ohms

FIGURE 4.8. Effect of contact orientation on the mutual coupling between the two contacts.

where c_1, c_2, c_3, c_4, c_5 and c_6 are process related constants whose values are given below for the TSMC 0.35 μm CMOS process.

$$c_1 = 2.006 \times 10^{-5} \, \Omega^{-1}(\mu m)^{-c_2} \qquad c_2 = 1.62$$

$$c_3 = 1.2 \times 10^{-5} \, \Omega^{-1}(\mu m)^{-c_4} \qquad c_4 = 1.3$$

$$c_5 = 1.008 \times 10^{-6} \, \Omega^{-1}(\mu m)^{-2} \qquad c_6 = 1.239 \times 10^{-3} \, \Omega^{-1}$$

For the model in Eq. (4.7), the sum of the lengths for the two contacts in the x and y directions are used. A third product term is included to improve the accuracy of the model. The error of α_{ij} values calculated using the model in Eq. (4.7) relative to the extracted values in Eq. (4.3) is shown in Figure 4.9. The maximum error is about 12% for all contact geometries.

Equation (4.7) does not consider the individual length of each contact. Different sizes for the two contacts can have the same sum of lengths in the x
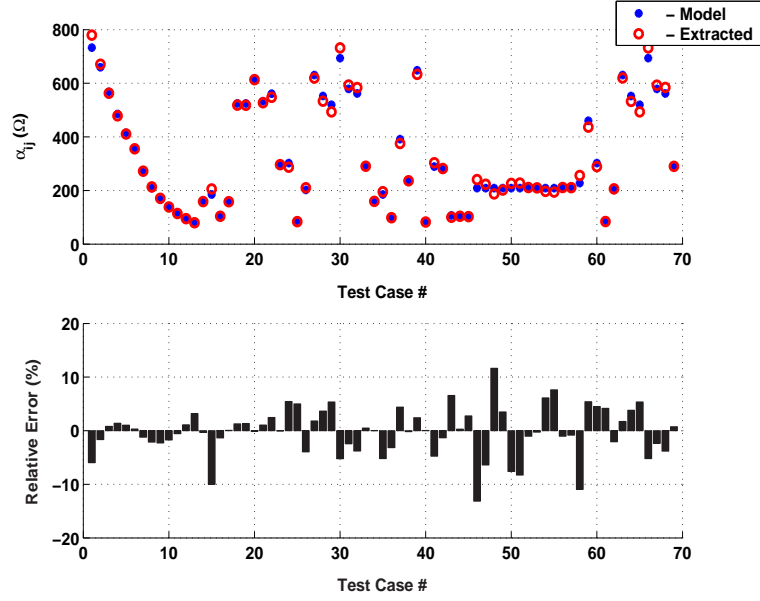
FIGURE 4.9. Accuracy of the α_{ij} model for all combinations of two contact geometries.

and y directions. This results in the same α_{ij} values according to the model. For example, let us consider two cases. In the first case, the two contacts sizes are 10 μm x 10 μm and 10 μm x 10 μm. In the second case, the two contact sizes are 18 μm x 2 μm and 2 μm x 18 μm. In both the cases, the sum of the lengths of the two contacts in the x and y directions is 20 μm. Using the model, we obtain the same α_{ij} value in both the cases.

The validity of this model against EPIC results needs to be evaluated. For this, 13 different two contact geometries were considered. The sum of the lengths of the two contacts in the x and y directions is the same for all the test cases, 20 μm in this example. Extracted values for α_{ij} using Eq. (4.3) are given in Table 4.1. As expected, α_{ij} calculated from the model in Eq. (4.7) is the same for all the test cases. The error in these values relative to the EPIC values is found to be within 15%.

TABLE 4.1. Accuracy of the model for limiting test cases with the same sum of the lengths and different individual lengths.

Contact 1 (μm x μm)	Contact 2 (μm x μm)	Lx_i+Lx_j (μm)	Ly_i+Ly_j (μm)	α_{ij} (Ω) extracted	α_{ij} (Ω) model	Relative Error (%)
10 x 10	10 x 10	20	20	213.56	209	2.13%
18 x 10	2 x 10	20	20	240.64	209	13.15%
15 x 10	5 x 10	20	20	223.26	209	6.39%
10 x 18	10 x 2	20	20	187.19	209	-11.65%
10 x 15	10 x 5	20	20	201.90	209	-3.52%
18 x 15	2 x 5	20	20	226.20	209	7.61%
18 x 5	2 x 15	20	20	227.83	209	8.27%
18 x 18	2 x 2	20	20	211.17	209	1.03%
18 x 2	2 x 18	20	20	209.56	209	0.27%
15 x 18	5 x 2	20	20	196.92	209	-6.14%
15 x 2	5 x 18	20	20	194.19	209	-7.62%
15 x 15	5 x 5	20	20	211.18	209	1.03%
15 x 5	5 x 15	20	20	210.71	209	0.81%

Another limitation of the model used for α_{ij} is that it does not have a one-to-one mapping between Lx and Ly for each contact. There is no differentiation when Ly_1 and Ly_2 are interchanged. For example, consider two cases. In the first case, the two contact sizes are 25 μm x 7 μm and 16 μm x 20 μm. In the second case, the two contact sizes are 25 μm x 20 μm and 16 μm x 7 μm. In both these cases, the α_{ij} value calculated using the model is the same.

Additionally, 10 new test cases were used by interchanging Ly_1 and Ly_2 in the existing test cases. These cases were simulated in EPIC and α_{ij} values were extracted using the model for Z_{ij}. Only 3 of these cases are shown in Table 4.2. In all 10 test cases, the extracted α_{ij} values with interchanged contact lengths are similar to the α_{ij} values obtained from the original contact sizes. The α_{ij} calculated using the model is the same for both the cases. The error from this model is within acceptable limits. Hence, the parameter α_{ij} can be modeled using the sum of lengths of the two contacts in the x and y axis for all contact geometries with acceptable error.

TABLE 4.2. Accuracy of the model for possibly limiting test cases where Ly_1 and Ly_2 are interchanged.

Test Case #	Contact 1 (μm x μm)	Contact 2 (μm x μm)	α_{ij} (Ω) extracted	α_{ij} (Ω) model	Relative Error (%)
1	10 x 16	3 x 3	286.78	302.39	-5.44%
	10 x 3	3 x 16	289.35	302.39	-4.50%
2	25 x 7	16 x 20	83.53	87.71	-5.00%
	25 x 20	16 x 7	84.20	87.71	-4.16%
3	18 x 14	3.6 x 2.5	210.24	201.92	3.96%
	18 x 2.5	3.6 x 14	206.18	201.92	2.07%

The next step is to develop a model for β_{ij}. β_{ij} values do not change much with contact sizes as shown in Figure 4.10. The sum of perimeters of the two contacts is sufficient to model this parameter very accurately. The model given by Eq. (4.8) matches the extracted values within 5% error as shown in Figure 4.10. The list of test structures includes cases where the sum of the perimeters

step process. First, Z_{ij} is modeled as a function of separation and secondly, the model parameters are modeled as a function of contact sizes. The accuracy can be increased by combining both the steps into a single step curve fitting. In this case, all three equations are used simultaneously and Z_{ij} is modeled as a function of separations and contact sizes. The process related constants c_i's obtained in this case are different from those of the two step process. The maximum error in Z_{ij} values is reduced to 15% because of the single curve fitting.

4.4. Model for y-separation

With the variation of Z_{ij} with d_x modeled accurately, the next step is to model the mutual coupling parameter Z_{ij} as a function of d_y.

4.4.1. Analysis of Simulation Results

Two identical square contacts of size 10 μm × 10 μm have been simulated for various d_y values from -100 μm to 100 μm. Since we are interested in modeling Z_{ij} as a function of d_y, the separation d_x is fixed at 20 μm. The resulting Z_{ij} values are plotted in Figure 4.11. As expected, the plot is symmetric about the point where d_y=0 when the centers of the two contacts along the y axis are aligned. The coupling decreases exponentially with separation and becomes negligible at large separations.

4.4.2. Model Development

As in Section 4.3.3, 60 different sets of two contact sizes have been simulated in EPIC. From the results, it is observed that Z_{ij} is of the order of 1-2 Ωs
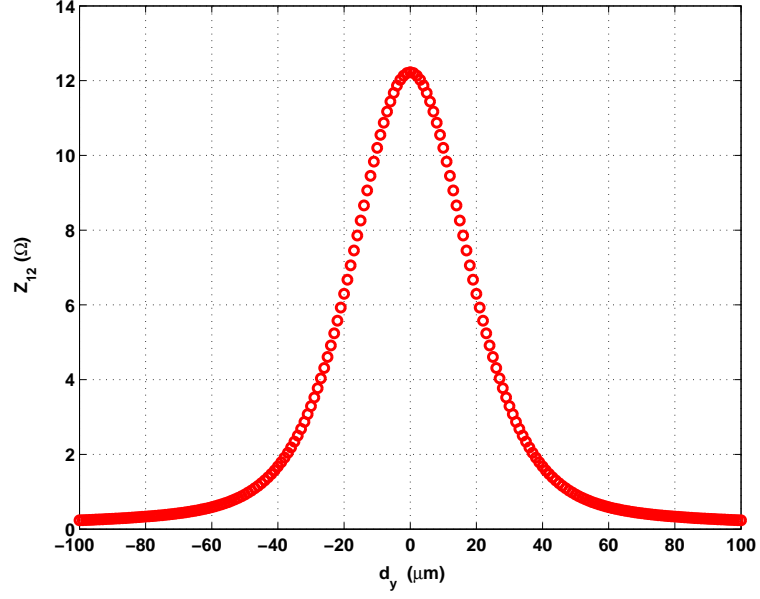
FIGURE 4.11. EPIC simulated values of Z_{ij} as a function of separation d_y.

for a separation $d_y = 40$ μm. As discussed in Section 4.3.2, the coupling between the two contacts can be neglected beyond this separation without much loss in the accuracy.

Since Z_{ij} has already been modeled as a function of x-separation d_x, the variation of Z_{ij} with respect to d_y needs to be modeled. The simulated values in Figure 4.11 can be normalized to the Z_{ij} value at $d_y=0$.

$$Z_{ij}^N(d_y) = \frac{Z_{ij}(d_x = d_{x0}, d_y)}{Z_{ij}(d_x = d_{x0}, d_y = 0\,\mu m)} \tag{4.9}$$

The cross coupling parameter Z_{ij} for any separation can be calculated as a product of the x-separation model and the y-separation model. At $d_y = 0$, $Z_{ij}^N(d_y)$ equals 1 and Z_{ij} reduces to the case analyzed in Section 4.3.

$$Z_{ij} = Z_{ij}(d_x) \times Z_{ij}^N(d_y) \tag{4.10}$$

A modified exponentially decaying function is used to model the Z_{ij} dependence on y-separation in Eq. (4.11). The model is symmetric about $d_y = 0$ as required. The model also satisfies the requirement that Z_{ij}^N equal 1 at $d_y = 0$. The parameter γ_{ij} is a function of the sizes of the two contacts. The model in Eq. (4.11) matches the simulated values within a 10% error bound. The comparison of the model and simulated values for Z_{ij}^N are shown in Figure 4.12 for 3 test cases.

$$Z_{ij}^N = exp(-\gamma_{ij}|d_y|^{1.5}) \tag{4.11}$$
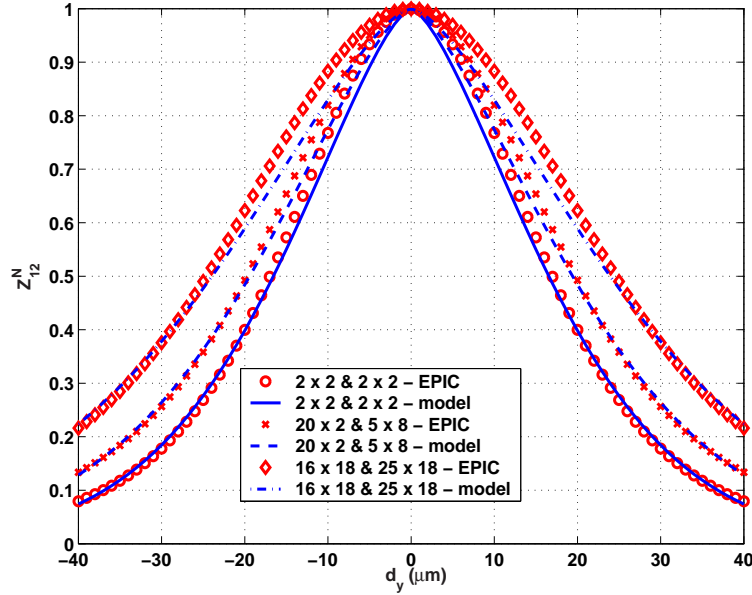
FIGURE 4.12. Comparison of the model of Z_{ij}^N with EPIC results.

The parameter γ_{ij} needs to be modeled as a function of the geometries of contact-i and contact-j. It is found that the sum of the perimeters of the two contacts is sufficient to develop an accurate model. Eq. (4.12) models the parameter γ_{ij} for all contact sizes within a 5% error bound as shown in Figure 4.13.

$$\gamma_{ij} = \frac{1}{c_9(P_i + P_j)^{c_{10}} + c_{11}} \tag{4.12}$$

where P_i and P_j are the perimeters of contact-i and contact-j, respectively and c_9, c_{10}, and c_{11} are process related constants whose values are given below for the TSMC 0.35 μm CMOS process.

$$c_9 = 0.14\,(\mu m)^{1.5-c_{10}} \qquad c_{10} = 1.26$$

$$c_{11} = 93.25\,(\mu m)^{1.5}$$
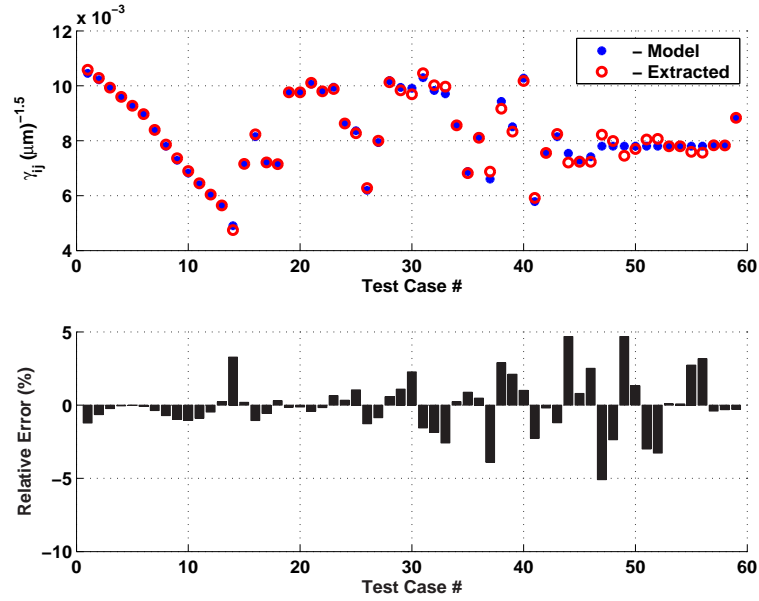
FIGURE 4.13. Accuracy of the γ_{ij} model for all combinations of two contact geometries.

Using the model of Eq. (4.12) in Eq. (4.11) gives a maximum error of 12% in Z_{ij} values. The complete model for the mutual coupling parameter for any contact size and separation between them is given by Eq. (4.13).

$$Z_{ij} = \alpha_{ij}\,exp(-\beta_{ij}\,d_x{}^{0.75}) \times exp(-\gamma_{ij}|d_y|^{1.5}) \qquad (4.13)$$

The mutual coupling parameter Z_{ij} is modeled using a total of 11 process related constants. There exists a trade-off between the accuracy of the model and the number of parameters. The model development and extraction of the

parameters are a one-time process for a given process technology. Once this information is obtained, the model can be applied to analyze the coupling between two contacts in an efficient and accurate manner.

In [11], it is assumed that Z_{ii} is a function of geometry of contact-i only. This assumption is not valid in all cases. Depending on sizes of contact-i and other surrounding contacts and the separations between them, the Z_{ii} can vary significantly. Even though, the Z_{ij} model is accurate at separations as small as 2 μm, the Z_{ii} model can give large error. Hence, the combined model can not be applied to test cases where the assumption of Z_{ii} is not valid.
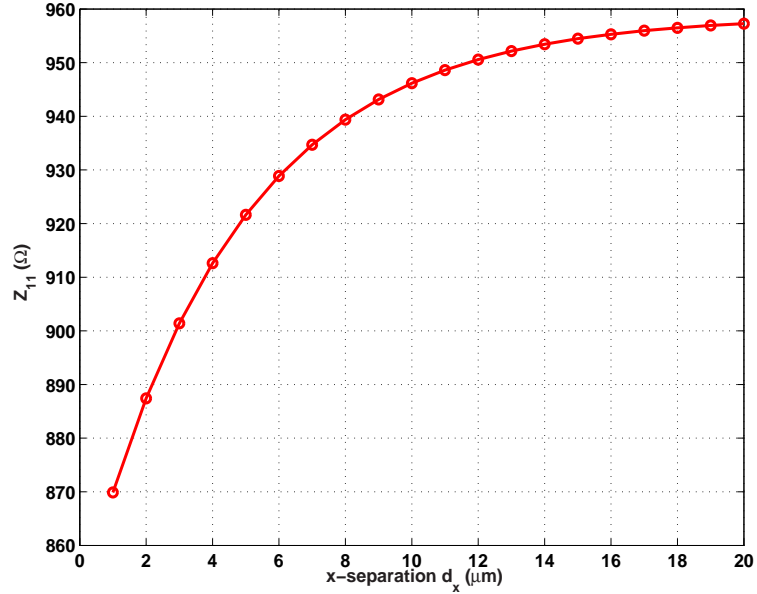
FIGURE 4.14. Variation of Z_{ii} at small separations.

In Figure 4.14, the variation of Z_{ii} of a 2 μm x 2 μm contact due to the presence of other contact of size 100 μm x 100 μm is shown as a function of separation between them. Few other combinations of two contact geometries are simulated and the results are summarized in Table 4.3.

TABLE 4.3. Variation of Z_{ii} at small separations.

Contact 1	Contact 2	Spacing for 2 % variation	Spacing for 5 % variation	Variation at 1 μm
(μm x μm)	(μm x μm)	(μm)	(μm)	
100 x 100	100 x 100	8	4.5	16%
100 x 100	2 x 2	-	-	0.02%
2 x 2	2 x 2	1.25	-	2.25%
2 x 10	2 x 10	3	-	4.5%
2 x 2	100 x 100	8	3.7	9%

5. VALIDATION OF THE MODEL

5.1. Two Contact Problems

To verify that the model is accurate, it has to be evaluated with contact geometries not used in extracting the model parameters. A set of 50 two contact problems with a wide range of dimensions and spacings are used. All these cases have been simulated in EPIC for varying separation along the x and y directions. The Z_{ij} values calculated from the model are within 15% of the EPIC results for these cases.

The separation is varied along one of the axes, either the x or the y axis. Also the two contacts are separated diagonally along the xy direction. The separations d_x and d_y are varied equally from 1 μm to 50 μm as shown in Figure 5.1. The entire set of 50 test structures were simulated in EPIC and the Z_{ij} values were obtained.
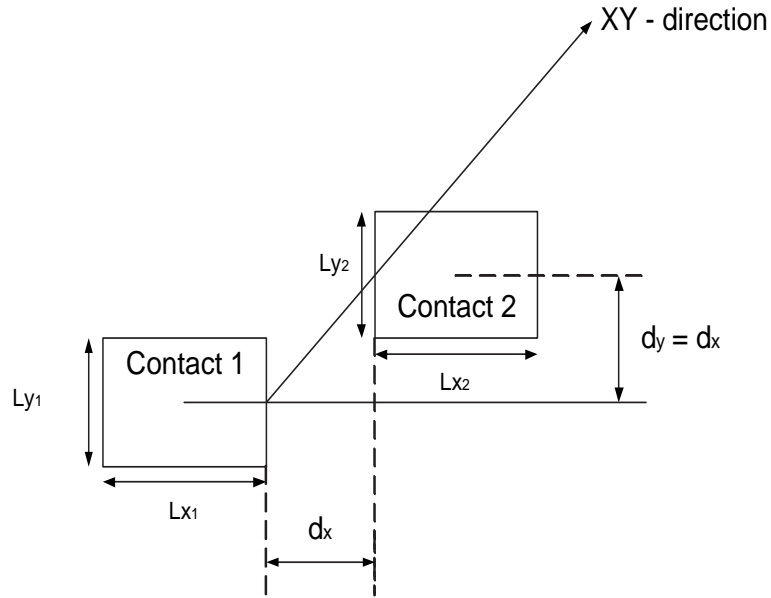

FIGURE 5.1. Varying the separation between two contacts along the XY direction.

Beyond a separation of 25 μm, the Z_{ij} values are in the order of few ohms. The coupling becomes negligible for separations greater than 25 μm and the accuracy of the model does not matter for these cases. The Z_{ij} values given by the model of Eq. (4.13) matches the simulated values within a 20% error bound for all the 50 test cases of which 3 are shown in Figure 5.2.
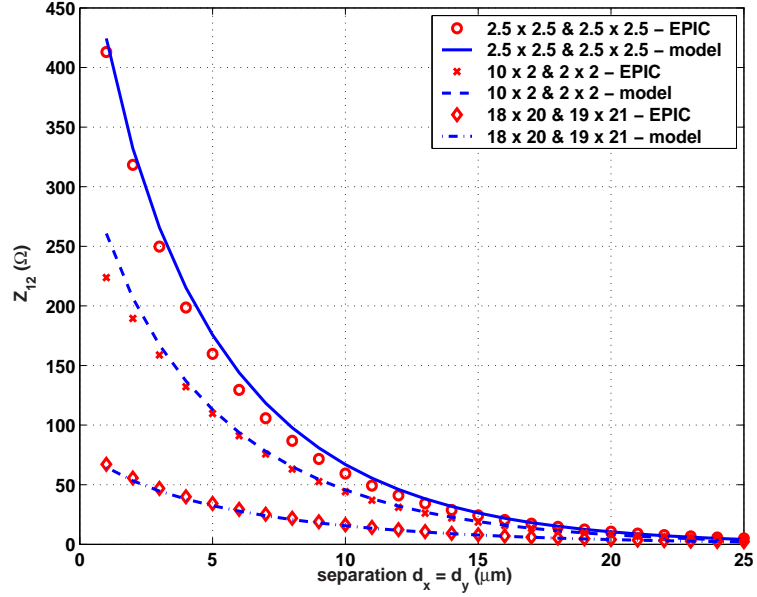
FIGURE 5.2. Model agrees with the EPIC results for separation along the XY direction.

The model is also validated with measured data. For two identical contacts 0.85 μm x 1.5 μm, the Z_{12} values from measurements are shown in Figure 5.3. The error from using the model is within 10% for separations greater than 2 μm.

5.2. Multi Contact Problem

So far we have discussed only the coupling between two contacts. In general, there will be more than two contacts. In fact, in a system-on-chip solution the substrate noise coupling between a large number of contacts has to be ana-
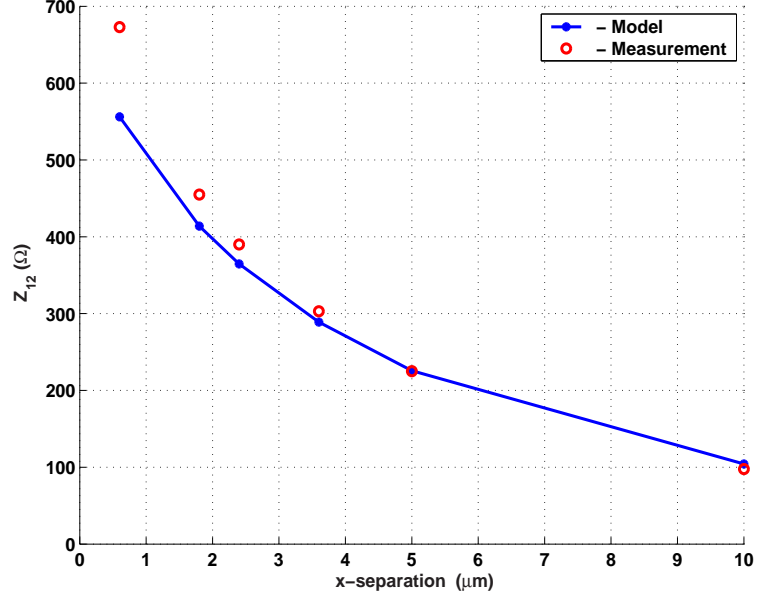
FIGURE 5.3. Model agrees with the measurement results.

lyzed. Since the coupling network is characterized using Z-parameters and the two-port Z-parameters are assumed to be independent of the presence of other contacts, the Z matrix for any N-contact problem can be obtained directly. All Z_{ii} and Z_{ij} entries of the $N \times N$ Z matrix are calculated using the model given in Eqs. (4.1) and (4.13), respectively. From the Z matrix, the resistance network can be computed as explained in Section 2.3.

The next objective is to evaluate how accurately and efficiently the model predicts the substrate noise coupling compared with the EPIC extractor.

Consider a 7-stage stepped buffer as a noise injecting block. Each stage is $e(=2.718)$ times larger than the preceeding stage. Also, each inverter is loaded by an additional inverter of the same size as the succeeding stage to have significant noise injection. The noise sensitive block is a folded cascode amplifier in a unity

gain feedback configuration. The circuit schematic for the two blocks is given in Figure 5.4. The two circuits are separated by about 140 μm in the layout.

Folded Cascode Opamp

Opamp Output

Substrate Coupling Network

DC Input

Stepped-Buffer

Interconnect Network

Digital Input CLK
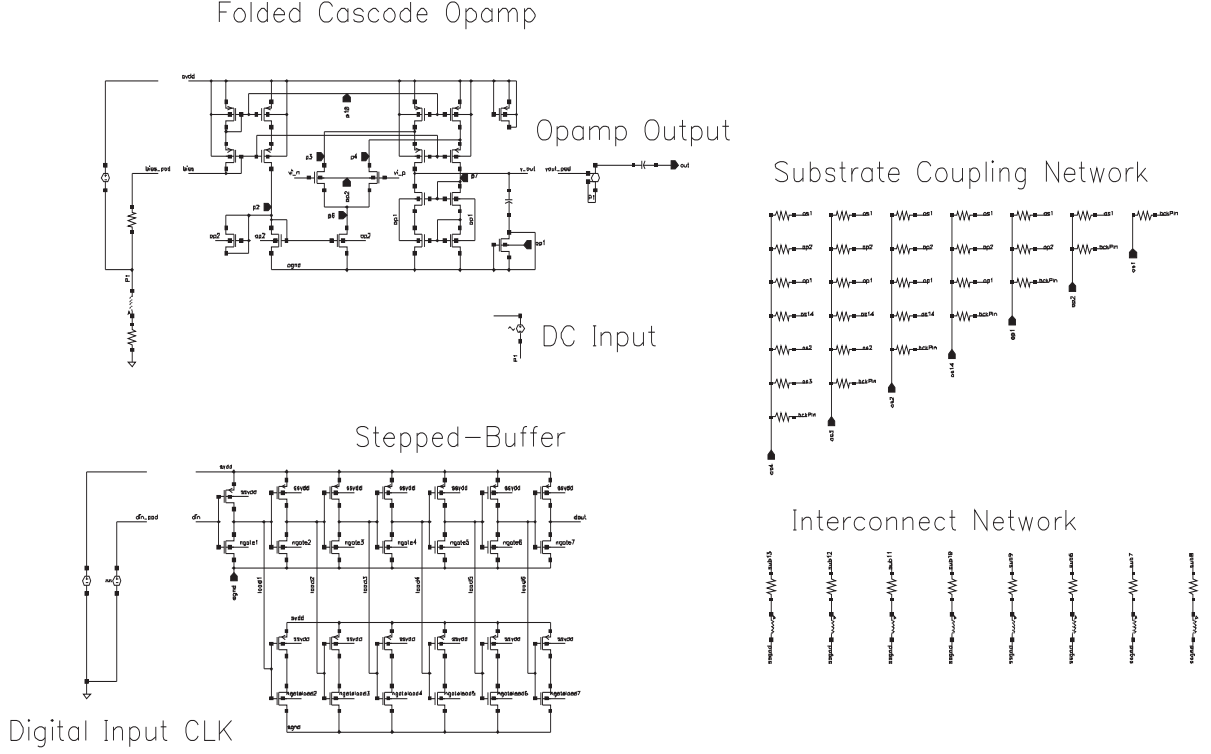
FIGURE 5.4. Schematic for analyzing substrate coupling between an opamp and a stepped buffer.

For this example there are a total of about 45 contacts. The coupling network is extracted using the Z parameter model and the EPIC extractor. The computation time for substrate network extraction using the model is less than a second as compared to 5 minutes using EPIC. The accuracy of the model in predicting some of the substrate resistances is shown in Table 5.1. As explained in Section 4.3.2, the smaller resistances match with higher accuracy. For large resistance values there are large errors due to the limitations of the model for large separations.

TABLE 5.1. Substrate resistance comparison between the model and EPIC.

EPIC Resistance (Ω)	Model Resistance (Ω)	Relative Error (%)
1.286 K	1.448 K	12.64
97.638 K	89.364 K	-8.47
530.645 K	427.22 K	-19.49
3.5 M	3.68 M	5.24
0.18 G	**0.39 G**	**112.05**
0.16 G	**16.64 T**	**-**

In practice, one is interested in analyzing the impact of substrate noise coupling on the performance of a sensitive circuit. The accuracy of the model has to be evaluated for these cases. A transient analysis is carried out for this setup. To highlight the significance of accurate substrate parasitic extraction, the package parasitics have been removed in simulations for both the EPIC and model cases. The buffer is clocked at 1 MHz. Noise is injected at every transition into the substrate through capacitive coupling. The amplifier has a DC input. In the absence of substrate noise, the output stays at the input voltage. However, in the presence of noise the amplifier picks up the noise from the substrate and these appear as spikes at the output of the amplifier. The results for a transient analysis are shown in Figure 5.5. From this figure, it can be seen that the model is in good agreement with the EPIC simulation results. These simulations also validate the assumption that large errors in high impedance values do not affect the final results.

For this example, only the coupling between NMOS transistors is considered and the coupling from the PMOS transistors is neglected. This is a valid
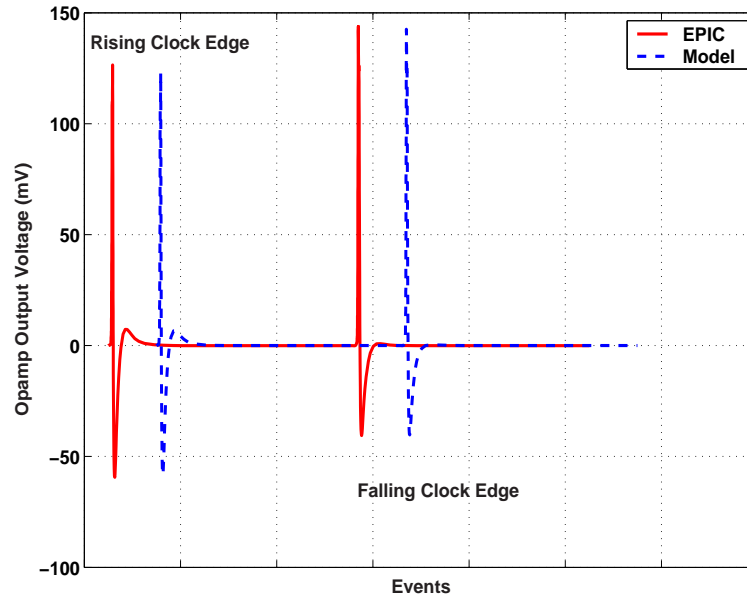
FIGURE 5.5. Comparison of transient substrate coupling between model and EPIC.

assumption as the noise from PMOS transistors couples through the n-well to p-substrate capacitance. The largest value of this capacitor in this particular example is in the order of femto Farads. The impedance offered by this capacitor becomes comparable to the substrate resistances only at frequencies above 2 GHz. Hence the coupling from the PMOSFETs can be neglected without much loss of accuracy.

6. CONCLUSIONS

Models are required to analyze substrate noise coupling in an efficient manner. The accuracy of these models depends on the assumptions and approximations made during the development phase. Accurate models can be developed by a careful analysis of numerical simulation results or measured data.

In this work, a Z-parameter based modeling approach is adopted because of its simplicity and generality to multiple contacts. The ratio-acceleration technique is employed to simplify the model whereby small Z_{ij} entries can be neglected. This affects only the cross coupling resistors and does not affect the final substrate noise coupling analysis.

Parametric models, scalable with contact geometries and separations, have been developed by curve fitting to EPIC results. Possible limitations of the model have been analyzed and the accuracy is found to be within the tolerable limits. The mutual coupling parameter Z_{ij} is modeled using 11 process related parameters.

Finally, the model is applied to a multi contact problem containing an analog and digital block. The model is very accurate for low impedances which provide the path for significant noise coupling. Whereas some of the high impedance path have large errors, they do not affect the final results. A transient analysis of substrate noise coupling for a circuit example gives the same result as EPIC.

BIBLIOGRAPHY

[1] B. R. Stanisic, N. K. Verghese, D. J. Allstot, R. A. Rutenbar and L. R. Carley, "Addressing substrate coupling in mixed-mode ICs: simulation and power distribution synthesis," *IEEE Journal of Solid-State Circuits*, pp. 226-237, March 1994.

[2] F. J. R. Clement, E. Zysman, M. Kayal and M. Declercq, "LAYIN: Toward a global solution for parasitic coupling modeling and visualization," in *Proc. IEEE Custom Integrated Circuit Conference*, May 1994, pp. 537-540.

[3] A. Samavedam, A. Sadate, K. Mayaram, and T. S. Fiez, "A scalable substrate noise coupling model for design of mixed-signal IC's," *IEEE Journal of Solid-State Circuits*, pp. 895–904, June 2000.

[4] A. J. van Genderen, N. P. van der Meijs and T. Smedes, "Fast computation of substrate resistances in large circuits," in *Proc. European Design and Test Conference*, March 1996, pp. 560-565.

[5] E. Charbon, R. Gharpurey, P. Miliozzi, R. G. Meyer and A. S. Vincentelli, *Substrate Noise: Analysis and Optimization for IC Design*, Kluwer Academic Publishers, 2001.

[6] C. G. Xu, "EPIC: A program for extraction of substrate resistance with the Green's Function method," Department of ECE, Oregon State University, 2003.

[7] R. Gharpurey and E. Charbon, "Substrate coupling: modeling, simulation and design perspectives," in *Proc. of Quality Electronic Design*, March 2004, pp. 283-290.

[8] A. Sharma, "Predictive methodologies for substrate parasitic extraction and modeling in heavily doped CMOS sibstrates," *M. S. Thesis*, Oregon State University, Corvallis, OR, July 2003.

[9] S. Donnay and G. Gielen, *Substrate Noise Coupling in Mixed Signal ASICs*, Kluwer Academic Publishers, 2003.

[10] N. K. Verghese, T. J. Schmerbeck and D. J. Allstot, *Simulation Techniques and Solutions for Mixed Signal Coupling in ICs*, Kluwer Academic Publishers, 1995.

[11] D. Ozis, "An efficient modeling approach for substrate noise coupling analysis with multiple contacts in heavily doped CMOS processes," *M. S. Thesis*, Oregon State University, August 2001.

[12] N. K. Verghese, "Extraction and simulation techniques for substrate coupled noise in mixed-signal ICs," *Ph. D dissertation*, Carnegie Mellon University, August 1995.

[13] A. J. Sinclair and J. A. Ferreira, "Analysis and design of transmission line structures by means of the geometric mean distance," in *IEEE AFRICON*, September 1996, pp. 1062-1065.

[14] H. Lan, T. W. Chen, C. O. Chui, and R. W. Dutton, "Compact modeling and experimental verification of substrate resistance in lightly doped substrates," in *SASIMI 2004*, October 2004, pp. 189–195.

[15] C. G. Xu, personal communications.

[16] P. Dewilde and Z. Q. Ning, *Models for Large IC*, Kluwer Academic Publishers, 1990.

[17] D. K. Su, M. J. Loinaz, S. Masui and B. A. Wooley, "Experimental results and modeling techniques for a substrate noise in mixed-signal ICs," *IEEE Journal of Solid-State Circuits*, pp. 420-430, April 1993.

[18] S. Kristiansson, S. P. Kagganti, T. Ewert, F. Ingvarson, J. Olsson and K. O. Jeppson, "Substrate resistance modeling for noise coupling analysis," in *IEEE Int. Conf. on Microelectronic Test Structures*, March 2003, pp. 124-129.

[19] H. Lan and R. W. Dutton, "Synthesized compact models of substrate noise coupling analysis and synthesis in mixed-signal ICs, " in *DATE 2004*, February 2004, pp. 836-841.

APPENDICES

APPENDIX A. List of test structures used to test the suitability of GMD

TABLE A-1. Dimensions of the test structures used to test the GMD.

Test Case Number	Contact 1 (μm X μm)	Contact 2 (μm X μm)
1	10 x 10	10 x 10
2	20 x 2	3 x 24
3	10 x 10	2 x 2
4	4 x 7	6 x 8
5	20 x 2	5 x 5
6	4 x 16	3 x 3
7	20 x 2	18 x 3
8	3 x 25	4 x 20